



HAL
open science

Impaired Activated/Memory Regulatory T Cell Clonal Expansion Instigates Diabetes in NOD Mice

Vanessa Mhanna, Gwladys Fourcade, Pierre Barennes, Valentin Quiniou, Hang P Pham, Paul-Gydeon Ritvo, Faustine Brimaud, Bruno Gouritin, Guillaume Churlaud, Adrien Six, et al.

► **To cite this version:**

Vanessa Mhanna, Gwladys Fourcade, Pierre Barennes, Valentin Quiniou, Hang P Pham, et al.. Impaired Activated/Memory Regulatory T Cell Clonal Expansion Instigates Diabetes in NOD Mice. *Diabetes*, 2021, 70 (4), pp.976-985. 10.2337/db20-0896 . hal-03263428

HAL Id: hal-03263428

<https://hal.sorbonne-universite.fr/hal-03263428>

Submitted on 17 Jun 2021

HAL is a multi-disciplinary open access archive for the deposit and dissemination of scientific research documents, whether they are published or not. The documents may come from teaching and research institutions in France or abroad, or from public or private research centers.

L'archive ouverte pluridisciplinaire **HAL**, est destinée au dépôt et à la diffusion de documents scientifiques de niveau recherche, publiés ou non, émanant des établissements d'enseignement et de recherche français ou étrangers, des laboratoires publics ou privés.

1 **Impaired activated/memory regulatory T cell clonal expansion instigates**
2 **diabetes in NOD mice**

3

4 Vanessa Mhanna^a, Gwladys Fourcade^a, Pierre Barennes^a, Valentin Quiniou^{a,b}, Hang P.
5 Pham^c, Paul-Gydeon Ritvo^a, Faustine Brimaud^a, Bruno Gouritin^a, Guillaume Churlaud^{a,b},
6 Adrien Six^{a,1}, Encarnita Mariotti-Ferrandiz^{a,1}, David Klatzmann^{a,b,1*}

7

8 ^aSorbonne Université, INSERM, Immunology-Immunopathology-Immunotherapy (i3),
9 F-75005 Paris, France.

10 ^bAP-HP, Hôpital Pitié-Salpêtrière, Biotherapy (CIC-BTi) and
11 Inflammation-Immunopathology-Biotherapy Department (i2B), F-75013, Paris, France.

12 ^cILTOO Pharma, Statistics Department, Paris, France.

13 ¹co-senior authors

14 *corresponding author

15 **Email:** david.klatzmann@sorbonne-universite.fr

16 **Phone number:** +33 1 42 17 74 60

17

18 **Word count:** 3994

19 **Number of figures:** 5

20 **Keywords**

21 Tolerance, immune regulation, immunopathology, immunotherapy, systems biology

22

23 **Abstract**

24 Regulatory T cell (Treg) insufficiency licenses the destruction of insulin-producing
25 pancreatic β cells by auto-reactive effector T cells (Teffs), causing spontaneous
26 autoimmune diabetes in non-obese diabetic (NOD) mice. We investigated the
27 contribution to diabetes of the TCR repertoires of naive regulatory T cells (nTregs),
28 activated/memory Tregs (amTregs), and $CD4^+$ Teffs from prediabetic NOD mice and
29 normal C57BL/6 (B6) mice. NOD mice amTreg and Teff repertoire diversity was
30 unexpectedly higher than that of B6 mice. This was due to the presence of highly
31 expanded clonotypes in B6 amTregs and Teffs that were largely lost in their NOD
32 counterparts. IL-2 administration to NOD mice restored such amTreg clonotype
33 expansions and prevented diabetes development. In contrast, IL-2 administration only led
34 to few or no clonotype expansions in nTregs and Teffs, respectively. Noteworthy, IL-2
35 expanded amTreg and nTreg clonotypes were markedly enriched in islet-antigen specific
36 TCRs. Altogether, our results highlight the link between a reduced clonotype expansion
37 within the activated Treg repertoire and the development of an autoimmune disease. They
38 also indicate that the repertoire of amTregs is amenable to rejuvenation by IL-2.

39 Non-obese diabetic (NOD) mice spontaneously develop autoimmune diabetes due to the
40 destruction of insulin-producing β cells by auto-reactive CD4⁺ and CD8⁺ T cells (1).
41 Diabetes susceptibility in NOD mice is attributed to genetic defects encoded by the
42 insulin-dependent diabetes (idd) loci including over 40 genes, among which the MHC
43 class II and interleukin-2 (IL-2) genes have major contributions to the pathophysiological
44 immune response leading to diabetes (2). The unique I-A^{g7} MHC-II molecule expressed
45 by NOD mice has been reported to bind certain peptides with low affinity, thus impairing
46 the thymocyte negative selection process (3,4). Reduced IL-2 production by activated
47 effector T cells (Teffs) was found in NOD mice and linked to an impairment of Treg
48 numbers and functionality (5-7). An increased diabetes incidence was observed in NOD
49 mice bearing an IL-2 alpha receptor subunit with reduced affinity for IL-2, which was
50 associated with a Treg but not a Teff defect (8). Likewise, the administration of low-dose
51 IL-2 to NOD mice promotes Treg expansion and activation, prevents diabetes onset and
52 even cures diabetic mice (9, 10). Thus, the altered tolerance promoting diabetes in NOD
53 mice could be the result of (i) a defect in thymic selection of Treg and Teff T-cell
54 receptor (TCR) repertoires and/or (ii) an altered Treg fitness due to IL-2 deprivation.

55 Previous studies of the TCR repertoires of NOD mice and type 1 diabetes patients yielded
56 inconsistent results. Some studies showed a restricted TRBV and TRBJ chain usage by
57 CD4⁺ T cells from pancreatic islets and pancreatic lymph nodes (PLN), indicating that
58 overrepresented islet-specific TCRs preferentially express certain TRBVJ genes (11–13).
59 Conversely, others showed a rather diverse gene usage among islet-infiltrating CD4⁺ T
60 cells in NOD mice (14), including islet-infiltrating memory CD4⁺ T cells (15, 16), and no
61 common highly used TRBVBJ combinations in T cells from PLN of type 1 diabetes

62 patients (17). Moreover, NOD Tregs were found to have a restricted TRA repertoire and
63 limited overlap with thymic CD4⁺ T cells (18, 19), while we found similar TRB diversity
64 between NOD peripheral Tregs and Teffs (20). These somehow conflicting results can be
65 explained by the fact that (i) most of these studies were performed on unsorted CD4⁺ T
66 cells and thus did not distinguish between regulatory and effector populations and/or (ii)
67 most Treg repertoire analyses were done on a limited fraction of the repertoire by using
68 TCR transgenic NOD mice or by focusing on few rearrangements (18, 19). More
69 importantly, most studies have overlooked the existence of regulatory T cell subsets.
70 Indeed, we previously showed that Tregs could be phenotypically divided into
71 CD4⁺Foxp3⁺CD44^{low}CD62L^{high} naïve Tregs (nTregs) that have a low turnover, and
72 CD4⁺Foxp3⁺CD44^{high}CD62L^{low} activated/memory Tregs (amTregs) that have a very
73 rapid turnover due to their interaction with their cognate antigens (21). In the healthy B6
74 mouse background, we showed that amTregs are enriched in deep tissue-draining lymph
75 nodes (LNs) and are characterized by unique clonotype expansions (22). Moreover, we
76 showed little overlap between amTreg and nTreg TRB repertoires (22). Thus, studying
77 amTreg and nTreg TCR repertoires without separating them may be confounding.
78 Here we compared the TCR repertoire of splenic amTregs, nTregs and Teffs of
79 prediabetic NOD and normal B6 mice to investigate whether and how an altered TCR
80 repertoire contributes to diabetes. We found that NOD amTregs have an unexpectedly
81 more diverse repertoire than that of B6 mice, due to the absence of expanded clonotypes.
82 Treatment of prediabetic NOD mice with IL-2, which prevents diabetes occurrence,
83 restored the expansion of clonotypes that are preferentially diabetes-reactive. Thus, the

84 TCR repertoire of amTregs is altered by an IL-2 insufficiency, which instigates diabetes
85 development in NOD mice, and is amenable to therapeutic recovery.

86 **Research Design and Methods**

87 **Study design**

88 Given the rarity of some of the studied cell subsets, we pooled the spleens of 6 to 8 young
89 mice matched for genetic background, age and sex. Six (three female and three male)
90 non-treated C57BL/6 or NOD pools of mice were used to study the repertoire at
91 homeostasis. Six young female NOD mice were treated with IL-2. Sample size was
92 determined for statistical significance and experimental feasibility. Investigators were not
93 blinded to the allocations during experiments and analyses.

94 **Mice**

95 Eight- to ten-week-old male and female C57BL/6- and NOD-Foxp3-EGFP transgenic
96 mice expressing green fluorescent protein (GFP) under the control of the Foxp3 gene
97 promoter were respectively provided by B. Malissen (Luminy, Marseille) and V.
98 Kuchroo (Brigham and Women's Hospital, Boston, MA). All animals were maintained at
99 the Sorbonne Université Centre d'Expérimentation Fonctionnelle animal facility under
100 specific pathogen-free conditions in agreement with the current European legislation on
101 animal care, housing and scientific experimentation (agreement number A751315). All
102 procedures were approved by the local animal ethics committee.

103 **IL-2 treatment**

104 Recombinant AAV8 vectors were produced as described previously (9). Six female
105 NOD-Foxp3-EGFP mice were injected once intraperitoneally with 10^{11} of rAAVs diluted
106 in PBS at 6 weeks of age. Serum was collected two weeks post-injection and IL-2 levels
107 were measured using a mouse IL-2 ELISA (eBioscience) according to the manufacturer's
108 recommendations. Mice were sacrificed at nine weeks of age.

109 **Spleen retrieval and cell sorting**

110 Spleens were collected from euthanized mice and splenocytes were stained with anti-Ter-
111 119-biotin (BD Biosciences), -B220-biotin (eBioscience) and -CD11c-biotin
112 (eBioscience) antibodies for 20 min at 4°C and labeled with anti-biotin magnetic beads
113 (Miltenyi Biotec) for 15 min at 4°C. B cells, erythrocytes and monocytes were depleted
114 on an AutoMACS separator (Miltenyi Biotec) following the manufacturer's procedure.
115 Enriched T cells were stained for 20 min at 4°C with the following monoclonal
116 antibodies at predetermined optimal dilutions: CD3-APC (BD Biosciences), CD4-
117 Horizon-V500 (BD Biosciences), CD8-Alexa-700 (BD Biosciences), CD44-PE (BD
118 Biosciences) and CD62L-eFluor-450 (eBioscience) and sorted on a FACSAria II
119 cytometer (BD Biosciences) with a purity > 95% into the following subsets: CD4⁺
120 FoxP3⁺ CD62^{low} CD44^{high} (activated/memory Tregs (amTregs)), CD4⁺ FoxP3⁺ CD62^{high}
121 CD44^{low} (naive Tregs (nTregs)) and CD4⁺ FoxP3⁻ (T effector cells (Teffs)). 1.10^5 to 5.10^6
122 sorted cells were stored in RNAqueous kit lysis buffer (Invitrogen) at -80 °C.

123 **cDNA library preparation for TR sequencing**

124 RNA was extracted using the RNAqueous Total RNA Isolation Kit (Invitrogen). TRB
125 libraries were prepared on 100 ng of RNA with the SMARTer Mouse TCRA/b Profiling
126 Kit (TakaraBio) and sequenced with HiSeq 2500 single read (300 bp) (Illumina) + 10%
127 PhiX at the “LIGAN Genomics platform” (23).

128 **Raw read processing**

129 Raw data in FASTQ format were processed for TRB sequence annotation using MiXCR
130 software (v.3.0.3) (24), which ensures PCR and sequencing error corrections and
131 provides for each sample a list of unique amino acid TRBs and their corresponding
132 counts. Annotated sequences were then analyzed using an in-house workflow to eliminate
133 long amino acid CDR3 sequences (length higher than the mean + 8). The resulting
134 datasets are summarized in Table S2.

135 **Data analysis**

136 *Statistical comparison*

137 Sample overlap was tested by computing the Jaccard distance (25) using the “vegan” R
138 package and plotted into a heatmap using the “pheatmap” package (26). Clustering
139 analysis was performed using the ‘Ward’ method. Principal component analysis was
140 performed using the “stats” R package. Renyi entropy (27) was calculated using “vegan”
141 and represents the distribution of clonal expansions as a function of the parameter *alpha*.
142 Probability density plots were plotted using the “ggplot2” R package (28).

143 *Network analysis*

144 For each cell population, the following method was adopted: The top most frequent 1000
145 CDR3 amino acid sequences from each of the six B6 or NOD mice were pooled and the

146 mean frequency was calculated for every sequence. The list was then ordered
147 decreasingly and the first 1000 sequences were selected. A matrix of pairwise
148 Levenshtein distances (LD) between the CDR3s was computed and used to construct the
149 networks. In these networks, vertices (CDR3 sequences) are connected by edges (LD=1)
150 only if they differ by one amino acid (insertion/deletion/substitution). A connected cluster
151 is defined as a set of two or more vertices connected by edges. The clustering coefficient
152 of a node in a network quantifies how close its neighbors are to being a clique (a closed
153 cluster). The maximum value is 1 if every neighbor connected to the node A is also
154 connected to every other node within the neighborhood. The node size represents the
155 mean frequency of each CDR3 in the network.

156 Analyses were performed using R packages: “stringdist” (29) was used to calculate LDs
157 and “Igraph” (30) to calculate network properties. Graphics visualization were done using
158 Cytoscape (31) and “ggplot2” for figures 3 and 5 respectively. In the latter, only clustered
159 nodes are represented and edges are not shown.

160 *Identification of expanded clonotypes*

161 In each sample, the first (Q1) and third (Q3) quartiles and the interquartile range (IQR)
162 were computed according to a negative binomial distribution fitted in the sequence read
163 counts, while excluding private clonotypes with a count of 1. Expanded clonotypes are
164 defined as those with counts greater than $Q3 + 1.5 \times IQR$.

165 *TCR Database*

166 Mouse CDR3 β s associated with diabetes (n=52), EAE (n=50), SLE (n=49) and cancer
167 (n=52) were collected from Friedman’s published database (32). These sequences were
168 derived from CD4⁺ T cells and identified by different methods including reactivity

169 assays, tetramer staining, selection of diabetes-specific TCRs following diabetes
170 induction and by sequencing of tumor T cell infiltrates in the context of cancer studies.

171 **Statistical analyses**

172 Statistical analyses were performed using the nonparametric Wilcoxon test with Holm
173 multiple testing correction using “ggpubr” R package (33). A p value of ≤ 0.05 was
174 considered statistically significant; * $p \leq 0.05$, ** $p \leq 0.01$, *** $p \leq 0.001$, **** $p \leq 0.0001$
175 and n.s. denotes not significant ($p > 0.05$). Mean percentage comparisons of diabetes,
176 EAE, SLE and cancer CDR3s were done using the Wilcoxon paired test with diabetes as
177 a reference group.

178 **Data availability**

179 Source data are provided in the manuscript and the Supplementary materials. Fastq data
180 were deposited in NCBI Sequence Read Archive repository under the BioProject ID
181 PRJNA635928.

182 **Results**

183 **Differences in repertoire composition between B6 and NOD**

184 We analyzed and compared the TCR beta chain (TRB) repertoire of splenic
185 CD4⁺Foxp3⁺CD44^{low}CD62L^{high} nTregs, CD4⁺Foxp3⁺CD44^{high} CD62L^{low} amTregs and
186 Foxp3⁻CD4⁺ Teffs in B6 and NOD mice.

187 Compared to B6 mice, flow cytometry showed a significant decrease in the NOD Treg
188 population ($p \leq 0.05$) associated with a decrease of amTreg proportions ($p \leq 0.01$) (Table
189 S 1). Cell numbers for each sorted population and their corresponding number of TRB
190 sequences and unique amino acid clonotypes are summarized in Table S2.

191 Principal component analysis of TRBVBJ usage, i.e. the frequency of each combination
192 in the repertoire irrespective of the clonotype abundance, clearly separated the genetic
193 backgrounds and the cell populations (Figure 1A). The first two components showed
194 different TRBVBJ usage between B6 and NOD mice, with the first component (PC1) that
195 separates the two genetic backgrounds explaining more than 68% of the variability. There
196 was also a clear difference between the cell populations from the same background, with
197 the two Treg subsets being close, but quite apart from Teffs. This reflects differences in
198 the combined generation frequency and survival through the thymic selection and
199 peripheral expansion of each generated TRBVBJ recombination.

200 To further investigate these differences, we assessed the clonotype (i.e. unique amino
201 acid TRBV-CDR3-TRBJ sequence) overlap between samples using the Jaccard distance
202 in which the higher the value, the more dissimilar the pair of samples compared (Figure
203 1B). Hierarchical clustering on the Jaccard scores accurately separated B6 from NOD
204 mouse samples. Surprisingly, within the latter cluster, amTregs are intermingled with
205 nTregs and Teffs, while, as expected from our previous study (22), amTregs clustered

206 separately in the B6 background. Overall, NOD mice display a peculiar repertoire
207 structure compared to B6 mice both at the TRB gene and clonotype level.

208 **Increased TCR diversity of Teffs and amTregs in NOD versus B6 mice**

209 We next explored the overall repertoire diversity at the clonotype level. We compared
210 cell populations and mouse backgrounds by calculating the Renyi entropy, which
211 evaluates diversity as a function of an *alpha* parameter (Figure 2A). The higher the *alpha*,
212 the higher is the weight put on frequent clonotypes. The higher the Renyi entropy, the
213 more diverse is the repertoire.

214 In B6 mice, nTregs have the most diverse repertoire while amTregs have the least diverse
215 one, and Teffs fall in between. In contrast, while nTregs in NOD mice have a repertoire
216 with a diversity similar to that in B6 mice, the diversities of the Teff and amTreg
217 repertoires are increased compared to B6 mice (Figure 2A). At *alpha*=0, for which the
218 Renyi index represents clonotype richness, no differences were observed between the B6
219 and NOD backgrounds (Figure 2B, left). This indicates that the overall richness of each
220 cell subset is not affected in NOD mice. At *alpha*=8, which gives more weight to
221 abundant clonotypes, Renyi indices were significantly higher in NOD amTregs and Teffs
222 than in the corresponding subsets in B6 mice (Figure 2B, right).

223 In view of these differences, we looked at the representativeness of the 100 most
224 predominant clonotypes within each repertoire. The cumulative percentages of the 100
225 most predominant clonotypes in B6 amTregs and Teffs were significantly higher than
226 their NOD counterparts (Figure 2C). This is due to the presence, in the B6 cell
227 populations, of highly frequent clonotypes depicted by blue lines which thickness is
228 proportional to their percentage in the repertoire (Figure 2D). In contrast, there were no
229 such clonotypes in B6 nor in NOD nTregs.

230 Collectively, these results reveal that a healthy naïve Treg repertoire is diverse with no
231 clonotype expansions. Conversely, the healthy amTreg repertoire, and to a lesser extent
232 the Teff repertoire, are enriched in clonotypes with high frequency, likely resulting from
233 antigen-driven expansions. In diabetes-prone NOD mice, such expansions are severely
234 reduced in amTregs and Teffs.

235 **Altered similarity structure of NOD amTreg and Teff repertoires**

236 Next, we examined the architecture of the repertoires. To this end, the 1000 most
237 frequent CDR3s per population were used to build similarity networks in which each
238 CDR3 (node) has a size proportional to its frequency and is connected by edges to other
239 CDR3s that differ to it by only one amino acid, i.e. having a Levenshtein distance of 1
240 (LD=1). This distance was shown to connect CDR3s that are likely to bind the same
241 peptide (34).

242 The structure of the nTreg repertoire appeared similar for B6 and NOD mice, made of
243 highly clustered CDR3s with low frequency (Figure 3A). In contrast, B6 amTreg
244 repertoire was mostly composed of individual or lightly connected with high frequencies,
245 reflecting polyclonal self-antigen-driven expansions (22,35). In accordance with the
246 previous observations (Figures 1 and 2), these expansions are much reduced in amTregs
247 from NOD mice. Similarly, node sizes of their Teffs appeared smaller than in B6 mice
248 (Figure 3A, middle).

249 Node frequency showed no differences for nTregs, a modest decrease for Teffs and a
250 marked decrease for amTregs in NOD mice compared to their counterparts in B6 mice
251 (Figure 3B). The clustering coefficient of each CDR3 within each network, which gives
252 an indication of the importance of these nodes in the global repertoire architecture,
253 showed no significant difference between NOD and B6 nTregs (Figure 3C). However,

254 significantly higher clustering coefficients were observed in Teffs and amTregs from
255 NOD compared to B6 mice.

256 Overall, the structural analysis of these networks highlights a higher sequence similarity
257 of Teff and amTreg CDR3s in NOD mice. As IL-2 production is notoriously low in NOD
258 mice and Tregs rely primarily on it for proliferation, we hypothesized that the reduced
259 amTreg expansions may result from an IL-2 shortage.

260 **Low dose IL-2 normalizes NOD amTreg repertoires**

261 As administration of IL-2 to NOD mice specifically enables the expansion of Tregs (9),
262 we investigated whether the abnormal repertoire diversity and structure of prediabetic
263 NOD mice could be restored by an IL-2 treatment. NOD mice were injected with an
264 adeno-associated virus coding for IL-2 (AAV-IL-2) that allows the continuous production
265 of IL-2 at low dose and prevents the occurrence of diabetes (9). As expected, total Treg
266 proportions increased significantly after IL-2 treatment (Figure 4A). Importantly, within
267 the Treg subsets, amTreg proportions showed a significant increase, at the expense of
268 nTregs (Figure 4A, Table S 3).

269 We next analyzed the expansions at the clonotype level after IL-2 treatment. To this end,
270 we identified expanded clonotypes as the ones showing counts greater than the
271 $Q3 + 1.5 \times IQR$ value, where Q3 is the third quartile and IQR the interquartile range of
272 sequence count distribution (see the Methods section and Table S 4). The abundance of
273 the expanded clonotypes from each sample was plotted in Figure 4B (left plots). Each
274 circle represents a clonotype whose size is proportional to its frequency in the repertoire.
275 amTregs and nTregs from AAV-IL-2-treated NOD mice were significantly enriched in
276 expansions compared to amTregs and nTregs from B6 or NOD mice. This is confirmed
277 by the density plots, which show that IL-2 treatment induces expansions of nTregs and

278 amTregs compared to their B6 and NOD counterparts, but not of Teffs (Figure 4B, right
279 plot). Thus, IL-2 administration restores amTreg clonotype expansions that were absent
280 in NOD mice.

281 **IL-2-expanded Tregs are enriched in diabetes-specific clonotypes**

282 We next examined whether the expanded clonotypes could be linked to diabetes. We
283 queried a published catalogue of TCRs with defined specificity (32). We identified a total
284 of 203 mouse CDR3 β amino acid sequences from CD4⁺ T cells associated with diabetes
285 (n=52), experimental autoimmune encephalomyelitis (EAE; n=50), systemic lupus
286 erythematosus (SLE; n=49) and cancer (n=52). We then searched for these sequences
287 within the expanded clonotypes and calculated their mean enrichment in each cell subset
288 (Figure 5A). Interestingly, diabetes-specific sequences showed higher expansions
289 compared to non-diabetes-specific sequences in nTregs and amTregs from IL-2-treated
290 NOD mice. There was also a modest enrichment of these sequences in B6 amTregs. To
291 further analyze the specificity pattern towards diabetes, we connected disease-specific
292 CDR3s by LD=1 to the pool of expanded amTreg and nTreg CDR3s. The number of
293 neighbors with LD=1 to diabetes-related sequences showed a significant increase
294 compared to other disease-specific CDR3s (Figure 5B).

295 Noteworthy, clonotypes identified as specific for islet antigens such as insulin and
296 glutamic acid decarboxylase by tetramer staining were detected in large clusters of IL-2
297 expanded clonotypes (Figure 5C, and Table S5).

298 **Discussion**

299 In this study, we report an altered amTreg TCR repertoire in NOD mice that can be
300 restored to normal by an IL-2 treatment. IL-2 expanded Tregs were enriched in

301 islet-antigen-specific TCRs and were associated with protection from diabetes. These
302 results have both heuristic and applied implications.

303 **The structure of the am- and n-Treg repertoires in a healthy mouse background**

304 In normal B6 mice, a control model that do not spontaneously develop any inflammatory
305 or autoimmune diseases, nTreg repertoires are very diverse, even more than those of
306 Teffs, with most clonotypes forming dense networks. These are the attributes of an
307 unmodified and tightly connected post-thymic selection repertoire (36). In contrast,
308 amTreg repertoires have a reduced diversity and are enriched in frequent clonotypes with
309 few connections. This illustrates the responses to distinct self-antigens, as expected from
310 a cell population that is constantly activated to control autoimmunity in numerous tissues.
311 Such similarity structures have also been described in the context of immunization and
312 aging (34).

313 In addition, amTreg repertoires show a higher overlap with each other than with nTregs
314 or Teffs, indicating that the self-antigens to which amTregs respond are shared between
315 individuals. This is also in agreement with our previous report of a low sequence overlap
316 between the two Treg subsets in the peripheral lymph nodes (22). The comparison with
317 Treg TRB repertoires from the NOD autoimmune-prone mouse strain strengthens this
318 conclusion. Reduction of amTreg major expansions is associated with disease
319 susceptibility, and their recovery with disease prevention.

320 Collectively, these results identify amTregs as the major subset involved in the
321 pathogenesis of autoimmunity and warrant separate analysis of amTregs and nTregs
322 when investigating their roles in health or disease.

323 **amTreg activation depends on IL-2**

324 The severe reduction in frequent clonotypes found in NOD mice, and their appearance
325 under IL-2 provision, highlight a major role of IL-2 in supporting amTreg survival.
326 NOD mice have a genetically determined IL-2 insufficiency, which is also reported in
327 human type 1 diabetes as well as in SLE and rheumatoid arthritis (37,38). It is thus likely
328 that the observed defect in amTreg fitness contributes to the pathophysiology of these
329 diseases. If so, the good news is that disease-relevant amTregs can be regenerated by IL-
330 2 treatment. We show herein that one injection of rAAV-IL-2 in prediabetic mice was
331 enough to expand NOD amTregs at the cell and repertoire levels. In our experiments, the
332 repertoire was analyzed 21 days after the initiation of treatment. As the approximate
333 duration of T cell differentiation in the thymus is of 28 days (39), newly generated
334 thymocytes are unlikely to contribute to the expanded clonotypes in the amTreg
335 population. Thus, the IL-2-induced amTregs most probably originate from peripheral
336 amTregs and/or nTregs that received their activation signal in the presence of IL-2. The
337 diabetes-related TCR expansions in both nTregs and amTregs further support that both
338 populations contribute to the restoration of a more balanced and complete disease-
339 relevant amTreg repertoire.

340 **Treg specificity to diabetes-related antigens**

341 The existence of public databases containing TCRs with known peptide specificities
342 allowed us to investigate the presence of antigen-specific sequences in our repertoires.
343 Diabetes-related CDR3s identified from the database were overrepresented in IL-
344 2-treated NOD Tregs and most connected in LD=1 networks, as shown by their high
345 number of neighbors. Linking the CDR3 similarity networks to annotated TCR datasets
346 was previously described by Madi et al., and showed that CDR3s with similar specificity

347 tend to cluster together (34). This indicates that diabetes-specific CDR3s could have core
348 motifs engaged in pancreatic antigen recognition, and shows the potential of such a tool
349 in identifying novel pathogenic TCRs. Indeed, repertoire analysis of islet-infiltrating T
350 cells revealed an accumulation of TCRs that were reactive in vitro to uncharacterized
351 autoantigens, distinct from the well-known glutamic acid decarboxylase and insulin
352 antigens (13).

353 These observations highlight a relationship between the specific expansion of pancreatic
354 antigen-related TCRs and the prevention of diabetes post IL-2 treatment.

355 **Contribution of I-A^{g7} to NOD pathophysiology**

356 It was hypothesized that diabetes development in NOD mice is associated with the
357 I-A^{g7} molecule that they express. Co-expression with a different type of MHC or
358 mutations within the I-A^{g7} molecule were shown to prevent insulinitis and diabetes (4, 40).

359 On the other hand, substitution of non-MHC regions from the C57BL/10 into the NOD
360 strain was sufficient to prevent insulinitis or diabetes, despite their expression of the I-A^{g7}
361 molecule (41). Our studies highlight the importance of non-MHC genes in diabetes onset
362 in the NOD mouse model. Indeed, we report here that IL-2 administration to pre-diabetic
363 NOD mice, previously shown to prevent the disease outcome, improves amTreg fitness.
364 This would argue that NOD Treg repertoires have the full potential to control
365 autoimmune responses, but fail to do so because an IL-2 deficiency impairs the amTreg
366 repertoire that can control islet autoreactivity.

367 However, our results do not exclude a potential enrichment of autoreactive T cells in the
368 NOD mice repertoire that would take the lead in the periphery where Tregs fail to
369 expand. In this regard, NOD mice have an overrepresentation of CDR3 β sequences

370 carrying hydrophobic amino acid doublets at positions 6 and 7 that have been shown to
371 confer high self-reactivity (42). Further studies of the TCR repertoire selection process in
372 the thymus of NOD mice should help address this important issue.

373 Altogether, our results reveal a link between a reduced expansion of clonotypes within
374 the activated Treg TCR repertoire and the development of an autoimmune disease.-IL-2
375 treatment not only activates Tregs, but also restores a repertoire of TCRs with relevant
376 specificities. Thus, our work indicates that fit amTregs are key to protection from
377 autoimmune diseases and highlights the value of studying these cells separately from the
378 whole Treg population. Importantly, amTreg repertoire abnormalities and restoration are
379 detected in the spleen, which affords a readout that is more representative of the
380 circulation than pancreatic lymph nodes and thus has a translational value. Our results
381 should guide further studies to elucidate the dynamics of pancreatic antigen-specific
382 amTregs in diabetic versus non-diabetic NOD mice, including in mice outside of a
383 pathogen-free environment, and identify TCR-based biomarkers of diabetes.

384

385 **Acknowledgments**

386 We thank F. Jebbawi and L. Barientos for their help in sample collection and cell sorting,
387 M. Mendez and N. Papaya for their help in RNA extraction and library preparations, and
388 K. El Soufi for his help in network analyses. We thank the staff of the animal care facility
389 for their excellent handling of mice. We also thank the UMR 8199 LIGAN-PM
390 Genomics platform (Lille, France) which belongs to the ‘Federation de Recherche’ 3508
391 Labex EGID (European Genomics Institute for Diabetes; ANR-10-LABX-46) and was
392 supported by the ANR Equipex 2010 session, for performing the sequencing of our
393 libraries.

394 **Funding**

395 This work was funded by the TRiPoD ERC-Advanced EU (No. 322856) and RHU iMAP
396 (ANR-16-RHUS-0001) grants to DK, with additional support from the Sorbonne
397 Université, INSERM and AP-HP. ILTOO pharma supported HPP.

398 **Author contributions**

399 VM, GF, PB, VQ, GC, FB, BG, P-GR and EM-F performed the experiments. VM
400 analyzed the data, with contributions from all authors. VM and HPP performed the
401 statistical analyses. VM, EM-F, AS and DK conceived the experiments. VM, AS, EM-F
402 and DK wrote the manuscript, with input from all authors. DK conceptualized and
403 supervised the study and is the guarantor for the contents of the article.

404 **Duality of interest**

405 DK is an investor of a patent related to the use of IL-2 in the treatment of autoimmune
406 diseases, owned by his public institution and licensed to ILTOO pharma, in which DK
407 has interests. The other authors declare no competing financial interests.

408

409 **References**

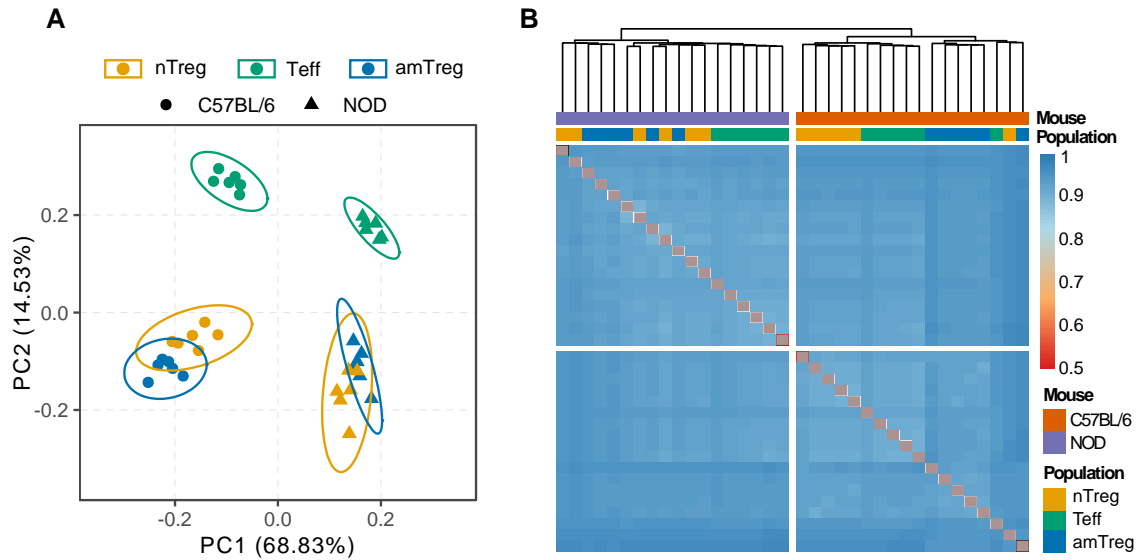
- 410 1. J. Verdaguer, D. Schmidt, A. Amrani, B. Anderson, N. Averill, P. Santamaria,
411 Spontaneous autoimmune diabetes in monoclonal T cell nonobese diabetic mice. *J. Exp.*
412 *Med.* **186**, 1663–1676 (1997).
- 413 2. Y.-G. Chen, C. E. Mathews, J. P. Driver, The Role of NOD Mice in Type 1 Diabetes
414 Research: Lessons from the Past and Recommendations for the Future. *Front.*
415 *Endocrinol.* **9**, 51 (2018).
- 416 3. O. Kanagawa, B. A. Vaupel, G. Xu, E. R. Unanue, J. D. Katz, Thymic positive
417 selection and peripheral activation of islet antigen-specific T cells: separation of two
418 diabetogenic steps by an I-A(g7) class II MHC beta-chain mutant. *J. Immunol.* **161**,
419 4489–4492 (1998).
- 420 4. T. Lund, L. O'Reilly, P. Hutchings, O. Kanagawa, E. Simpson, R. Gravely, P.
421 Chandler, J. Dyson, J. K. Picard, A. Edwards, D. Kioussis, A. Cooke, Prevention of
422 insulin-dependent diabetes mellitus in non-obese diabetic mice by transgenes encoding
423 modified I-A β -chain or normal I-E α -chain. *Nature.* **345**, 727–729 (1990).
- 424 5. D. Klatzmann, A. K. Abbas, The promise of low-dose interleukin-2 therapy for
425 autoimmune and inflammatory diseases. *Nature Reviews Immunology.* **15**, 283–294
426 (2015).
- 427 6. S. A. Long, K. Cerosaletti, P. L. Bollyky, M. Tatum, H. Shilling, S. Zhang, Z.-Y.
428 Zhang, C. Pihoker, S. Sanda, C. Greenbaum, J. H. Buckner, Defects in IL-2R signaling
429 contribute to diminished maintenance of FOXP3 expression in CD4(+)CD25(+)
430 regulatory T-cells of type 1 diabetic subjects. *Diabetes.* **59**, 407–415 (2010).
- 431 7. E. Sgouroudis, A. Albanese, C. A. Piccirillo, Impact of protective IL-2 allelic variants
432 on CD4+ Foxp3+ regulatory T cell function in situ and resistance to autoimmune diabetes
433 in NOD mice. *J. Immunol.* **181**, 6283–6292 (2008).
- 434 8. C. J. Dwyer, A. L. Bayer, C. Fotino, L. Yu, C. Cabello-Kindelan, N. C. Ward, K. H.
435 Toomer, Z. Chen, T. R. Malek, Altered homeostasis and development of regulatory T cell
436 subsets represent an IL-2R-dependent risk for diabetes in NOD mice. *Sci Signal.* **10**
437 (2017), doi:10.1126/scisignal.aam9563.
- 438 9. G. Churlaud, V. Jimenez, J. Ruberte, M. Amadoudji Zin, G. Fourcade, G. Gottrand, E.
439 Casana, B. Lambrecht, B. Bellier, E. Piaggio, F. Bosch, D. Klatzmann, Sustained
440 stimulation and expansion of Tregs by IL2 control autoimmunity without impairing
441 immune responses to infection, vaccination and cancer. *Clinical Immunology.* **151**, 114–
442 126 (2014).
- 443 10. M. Rosenzweig, G. Churlaud, R. Mallone, A. Six, N. Dérian, W. Chaara, R.
444 Lorenzon, S. A. Long, J. H. Buckner, G. Afonso, H.-P. Pham, A. Hartemann, A. Yu, A.
445 Pugliese, T. R. Malek, D. Klatzmann, Low-dose interleukin-2 fosters a dose-dependent

- 446 regulatory T cell tuned milieu in T1D patients. *Journal of Autoimmunity*. **58**, 48–58
447 (2015).
- 448 11. I. Marrero, A. Vong, Y. Dai, J. D. Davies, T cell populations in the pancreatic lymph
449 node naturally and consistently expand and contract in NOD mice as disease progresses.
450 *Molecular Immunology*. **52**, 9–18 (2012).
- 451 12. L. Li, Q. He, A. Garland, Z. Yi, L. T. Aybar, T. B. Kepler, J. A. Frelinger, B. Wang,
452 R. Tisch, Cell-Specific CD4⁺ T Cell Clonotypes in Peripheral Blood and the Pancreatic
453 Islets Are Distinct. *The Journal of Immunology*. **183**, 7585–7591 (2009).
- 454 13. F. J. Baker, M. Lee, Y. -h. Chien, M. M. Davis, Restricted islet-cell reactive T cell
455 repertoire of early pancreatic islet infiltrates in NOD mice. *Proceedings of the National
456 Academy of Sciences*. **99**, 9374–9379 (2002).
- 457 14. Nakano, T cell receptor V gene usage of islet beta cell-reactive T cells is not
458 restricted in non-obese diabetic mice. *Journal of Experimental Medicine*. **173**, 1091–1097
459 (1991).
- 460 15. I. Marrero, D. E. Hamm, J. D. Davies, High-Throughput Sequencing of Islet-
461 Infiltrating Memory CD4⁺ T Cells Reveals a Similar Pattern of TCR V β Usage in
462 Prediabetic and Diabetic NOD Mice. *PLoS ONE*. **8**, e76546 (2013).
- 463 16. I. Marrero, C. Aguilera, D. E. Hamm, A. Quinn, V. Kumar, High-throughput
464 sequencing reveals restricted TCR V β usage and public TCR β clonotypes among
465 pancreatic lymph node memory CD4⁺ T cells and their involvement in autoimmune
466 diabetes. *Molecular Immunology*. **74**, 82–95 (2016).
- 467 17. H. R. Seay, E. Yusko, S. J. Rothweiler, L. Zhang, A. L. Posgai, M. Campbell-
468 Thompson, M. Vignali, R. O. Emerson, J. S. Kaddis, D. Ko, M. Nakayama, M. J. Smith,
469 J. C. Cambier, A. Pugliese, M. A. Atkinson, H. S. Robins, T. M. Brusko, Tissue
470 distribution and clonal diversity of the T and B cell repertoire in type 1 diabetes
471 (2016),doi:10.1172/jci.insight.88242.
- 472 18. C. Ferreira, Y. Singh, A. L. Furmanski, F. S. Wong, O. A. Garden, J. Dyson, Non-
473 obese diabetic mice select a low-diversity repertoire of natural regulatory T cells.
474 *Proceedings of the National Academy of Sciences*. **106**, 8320–8325 (2009).
- 475 19. J. Kern, R. Drutel, S. Leanhart, M. Bogacz, R. Pacholczyk, Reduction of T Cell
476 Receptor Diversity in NOD Mice Prevents Development of Type 1 Diabetes but Not
477 Sjögren's Syndrome. *PLoS ONE*. **9**, e112467 (2014).
- 478 20. P.-G. Ritvo, A. Saadawi, P. Barennes, V. Quiniou, W. Chacara, K. El Soufi, B.
479 Bonnet, A. Six, M. Shugay, E. Mariotti-Ferrandiz, D. Klatzmann, High-resolution
480 repertoire analysis reveals a major bystander activation of Tfh and Tfr cells. *Proc Natl
481 Acad Sci USA*. **115**, 9604–9609 (2018).

- 482 21. S. Fisson, G. Darrasse-Jèze, E. Litvinova, F. Septier, D. Klatzmann, R. Liblau, B. L.
483 Salomon, Continuous activation of autoreactive CD4⁺ CD25⁺ regulatory T cells in the
484 steady state. *J. Exp. Med.* **198**, 737–746 (2003).
- 485 22. A.-S. Bergot, W. Chaara, E. Ruggiero, E. Mariotti-Ferrandiz, S. Dulauroy, M.
486 Schmidt, C. von Kalle, A. Six, D. Klatzmann, TCR sequences and tissue distribution
487 discriminate the subsets of naïve and activated/memory Treg cells in mice: Molecular
488 immunology. *European Journal of Immunology.* **45**, 1524–1534 (2015).
- 489 23. P. Barennes, V. Quiniou, M. Shugay, E. S. Egorov, A. N. Davydov, D. M. Chudakov,
490 I. Uddin, M. Ismail, T. Oakes, B. Chain, A. Eugster, K. Kashofer, P. P. Rainer, S. Darko,
491 A. Ransier, D. C. Douek, D. Klatzmann, E. Mariotti-Ferrandiz, Benchmarking of T cell
492 receptor repertoire profiling methods reveals large systematic biases. *Nat Biotechnol*
493 (2020)
- 494 24. D. A. Bolotin, S. Poslavsky, I. Mitrophanov, M. Shugay, I. Z. Mamedov, E. V.
495 Putintseva, D. M. Chudakov, MiXCR: software for comprehensive adaptive immunity
496 profiling. *Nature Methods.* **12**, 380–381 (2015).
- 497 25. P. Jaccard, Étude comparative de la distribution florale dans une portion des Alpes et
498 du Jura. *Imprimerie Corbaz & Comp.* (1901)
- 499 26. R. Kolde, pheatmap (2019).
- 500 27. R. Alfred, On measures of entropy and information. In: *Proceedings of the Fourth*
501 *Berkeley Symposium on Mathematical Statistics and Probability* (1961), pp. 547–61.
- 502 28. H. Wickham, D. Navarro, T. Lin Pedersen, *ggplot2: Elegant Graphics for Data*
503 *Analysis* (Springer, 2nd edition).
- 504 29. P.J. van der Loo, Mark, The stringdist Package for ApproximateString Matching. *The*
505 *R Journal.* Vol. 6/1, (2020)
- 506 30. G. Csardi, T. Nepusz, The igraph software package for complex network research
507 (2006).
- 508 31. P. Shannon, Cytoscape: A Software Environment for Integrated Models of
509 Biomolecular Interaction Networks. *Genome Research.* **13**, 2498–2504 (2003).
- 510 32. N. Tickotsky, T. Sagiv, J. Prilusky, E. Shifrut, N. Friedman, McPAS-TCR: a
511 manually curated catalogue of pathology-associated T cell receptor sequences.
512 *Bioinformatics.* **33**, 2924–2929 (2017).
- 513 33. Alboukadel, ggpubr R Package: ggplot2-Based Publication Ready Plots (2020)
- 514 34. A. Madi, A. Poran, E. Shifrut, S. Reich-Zeliger, E. Greenstein, I. Zaretsky, T. Arnon,
515 F. V. Laethem, A. Singer, J. Lu, P. D. Sun, I. R. Cohen, N. Friedman, T cell receptor
516 repertoires of mice and humans are clustered in similarity networks around conserved
517 public CDR3 sequences. *eLife.* **6** (2017), doi:10.7554/eLife.22057.

- 518 35. G. Darrasse-Jèze, A.-S. Bergot, A. Durgeau, F. Billiard, B. L. Salomon, J. L. Cohen,
519 B. Bellier, K. Podsypanina, D. Klatzmann, Tumor emergence is sensed by self-specific
520 CD44^{hi} memory Tregs that create a dominant tolerogenic environment for tumors in
521 mice. *Journal of Clinical Investigation* (2009)
- 522 36. Y. Elhanati, A. Murugan, C. G. Callan, T. Mora, A. M. Walczak, Quantifying
523 selection in immune receptor repertoires. *Proceedings of the National Academy of*
524 *Sciences*. **111**, 9875–9880 (2014).
- 525 37. G. D. Kitas, M. Salmon, M. Farr, J. S. Gaston, P. A. Bacon, Deficient interleukin 2
526 production in rheumatoid arthritis: association with active disease and systemic
527 complications. *Clin. Exp. Immunol.* **73**, 242–249 (1988).
- 528 38. K. S. Zier, M. M. Leo, R. S. Spielman, L. Baker, Decreased Synthesis of Interleukin-
529 2 (IL-2) in Insulin-dependent Diabetes Mellitus. *Diabetes*. **33**, 552–555 (1984).
- 530 39. V. Thomas-Vaslin, H. K. Altes, R. J. de Boer, D. Klatzmann, Comprehensive
531 Assessment and Mathematical Modeling of T Cell Population Dynamics and
532 Homeostasis. *J Immunol.* **180**, 2240–2250 (2008).
- 533 40. L. Gioia, M. Holt, A. Costanzo, S. Sharma, B. Abe, L. Kain, M. Nakayama, X. Wan,
534 A. Su, C. Mathews, Y.-G. Chen, E. Unanue, L. Teyton, Position β 57 of I-A^{g7} controls
535 early anti-insulin responses in NOD mice, linking an MHC susceptibility allele to type 1
536 diabetes onset. *Sci. Immunol.* **4**, eaaw6329 (2019).
- 537 41. D. V. Serreze, M. Bridgett, H. D. Chapman, E. Chen, S. D. Richard, E. H. Leiter,
538 Subcongenic Analysis of the Idd13 Locus in NOD/Lt Mice: Evidence for Several
539 Susceptibility Genes Including a Possible Diabetogenic Role for β 2-Microglobulin. *The*
540 *Journal of Immunology*. **160**, 1472–1478 (1998).
- 541 42. B. D. Stadinski, K. Shekhar, I. Gómez-Touriño, J. Jung, K. Sasaki, A. K. Sewell, M.
542 Peakman, A. K. Chakraborty, E. S. Huseby, Hydrophobic CDR3 residues promote the
543 development of self-reactive T cells. *Nature Immunology*. **17**, 946–955 (2016).
- 544

545 **Figures**



546

547

548 **Figure 1. B6 and NOD mice express different TCR repertoires. (A)** PCA biplot for

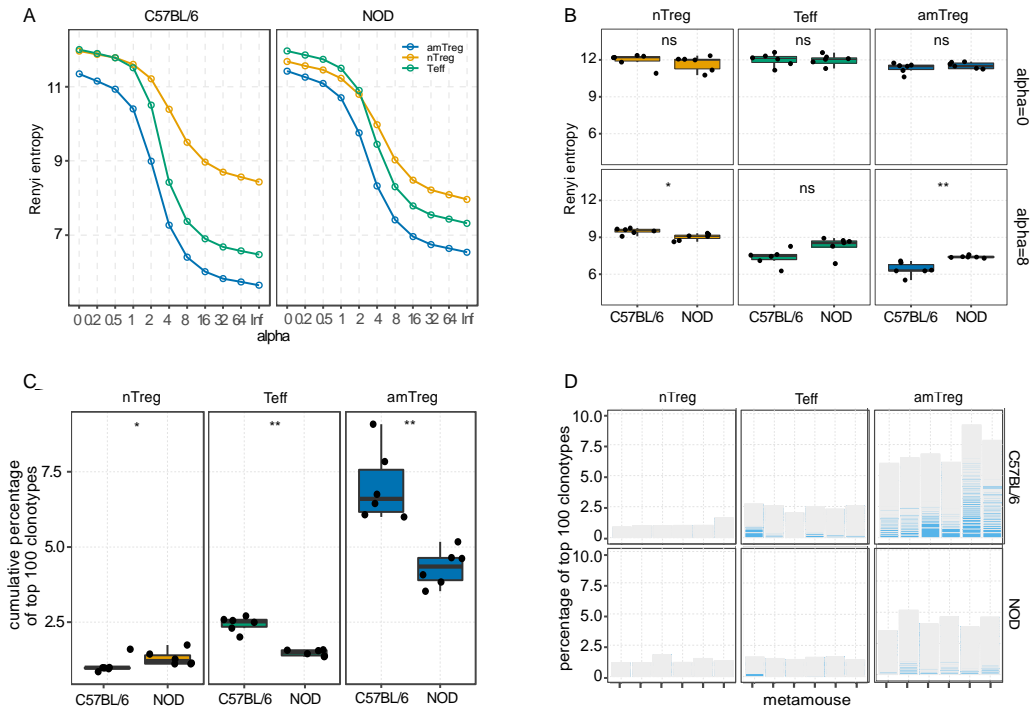
549 TRBVBJ usage of all B6 (dots) and NOD (triangles) samples. Cell populations are

550 identified based on their colors. **(B)** Heatmap of the pairwise Jaccard distances calculated

551 at the clonotype level. Scores range between 0 (complete similarity) and 1 (no similarity).

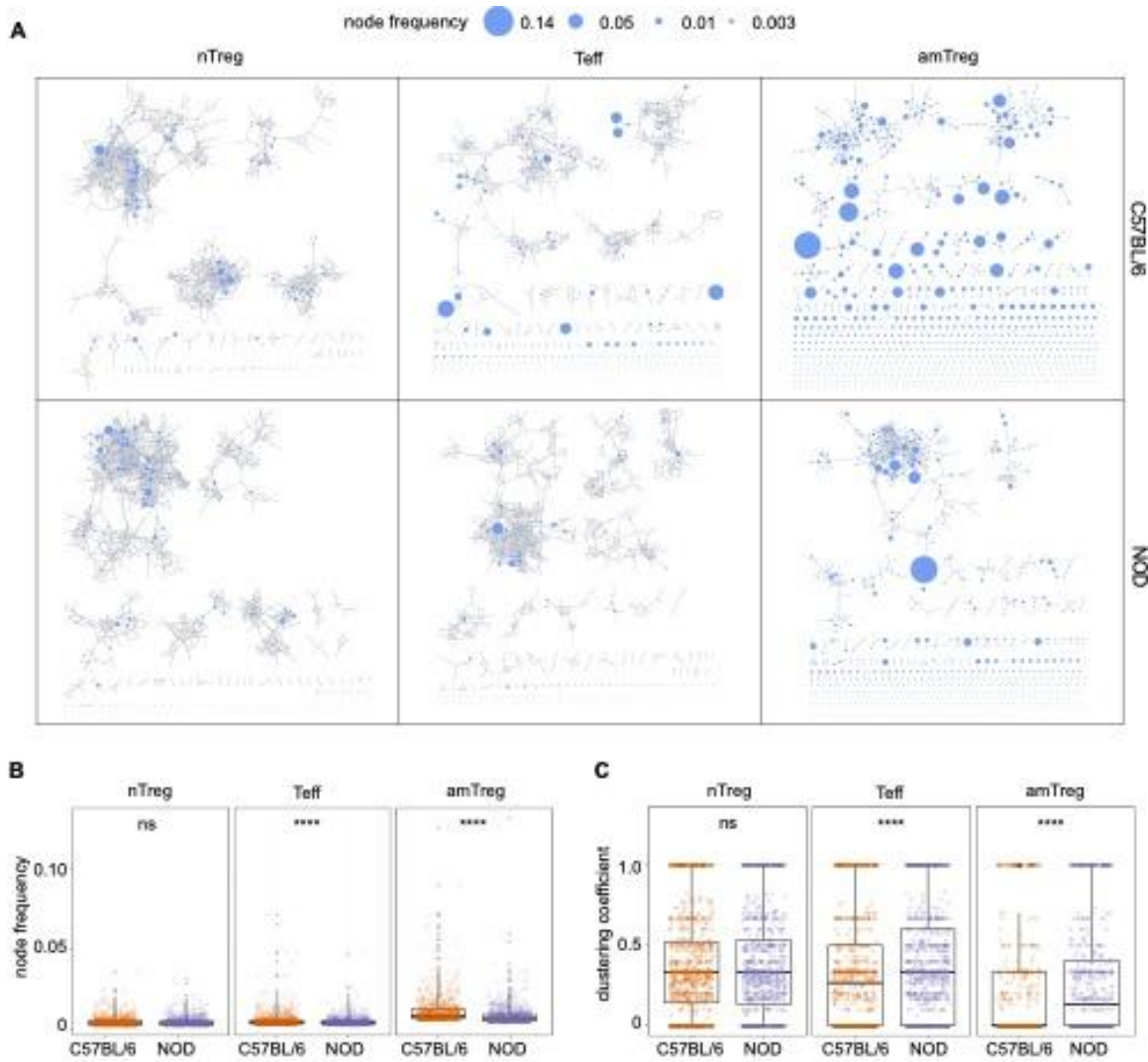
552 The hierarchical clustering was performed using Ward's method.

553



554

555 **Figure 2. Increased diversity of NOD Teffs and amTregs compared to B6.** (A) Renyi
 556 profiles for nTregs (yellow), CD4 Teffs (green) and amTregs (blue) in B6 and NOD
 557 mice. Points represent the mean of all six mice and shaded areas represent the standard
 558 error. (B) Renyi values were compared between B6 and NOD mice within each cell
 559 population at $\alpha = 0$ and $\alpha = 8$. (C) Mean cumulative percentage of the 100 most
 560 predominant clonotypes of the six mice for each cell population. (D) Percentage of the
 561 top 100 clonotypes within the three cell populations in B6 (upper plot) and in NOD
 562 (lower plot) backgrounds. Each blue line and its thickness represent a unique clonotype
 563 and its occurrence, grey “bars” are the stacking of slim grey lines representing rare
 564 clonotypes. (B, C) $n=6$, ns $P > 0.05$, * $P \leq 0.05$, ** $P \leq 0.01$, Wilcoxon test with Holm’s
 565 correction.



567

568

Figure 3. Similarity structure of nTreg, Teff and amTreg CDR3 repertoires. (A)

569

each cell population, the most frequent 1000 CDR3s across all mice were identified based

570

on their mean frequency and used to construct networks based on the Levenshtein

571

distance: CDR3 sequences (nodes) with one amino acid difference

572

(insertion/deletion/substitution) are connected by an edge. One network was constructed

573

per cell population and mouse background. **(B)** CDR3 frequency comparison between B6

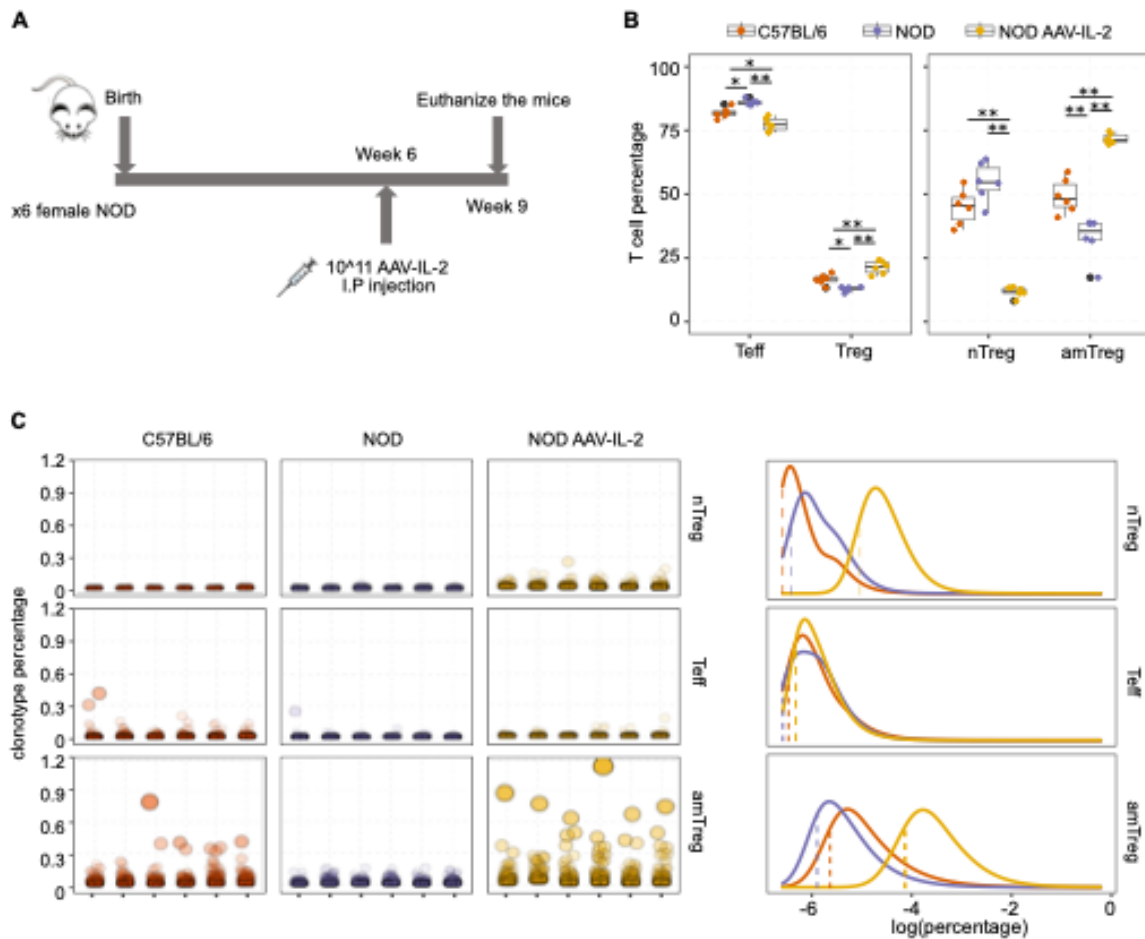
574

and NOD mice for each cell subset. **(C)** Comparison of the-clustering coefficient, which

575

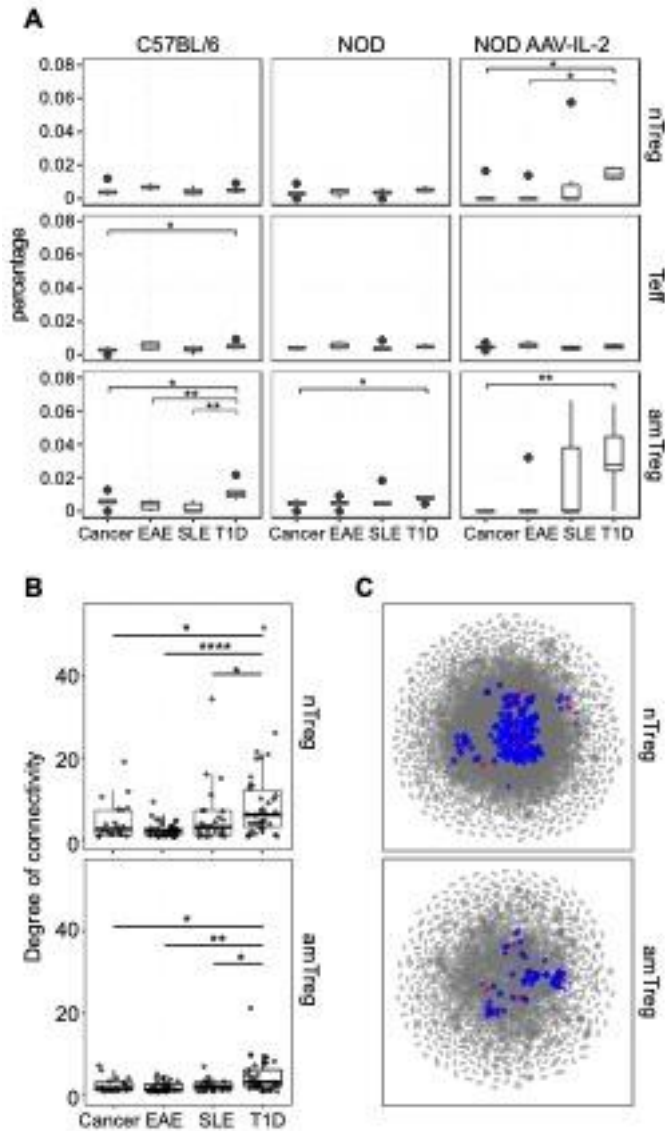
quantifies the degree to which neighbor nodes tend to cluster together, between B6 and

576 NOD mice in each cell subset. CDR3s with no connections are excluded. **(B, C)** Each dot
 577 represents a CDR3 and boxplots represent the median, first and third quartiles. ns $P >$
 578 0.05, *** $P \leq 0.001$, **** $P \leq 0.0001$, Wilcoxon test with Holm's correction.



579 **Figure 4. IL-2 induces Treg clonotype expansions.** **(A)** Experimental scheme. **(B)** Box
 580 plots show the percentage of T cells in each B6 (orange), NOD (purple) and IL-2–treated
 581 NOD (yellow) mice (n=6 per background). **(C, left plot)** The abundance (in %) of
 582 expanded clonotypes for each sample (each column represents a single sample) within the
 583 three populations and mouse backgrounds. Expanded clonotypes were identified as the
 584 ones with counts greater than $Q3 + 1.5 \times IQR$ according to a fitted negative binomial
 585

586 distribution. **(C, right plot)** Probability density plot based on the mean expanded
 587 clonotype distribution between the three mouse conditions for each cell subset. Colored
 588 dashed lines represent the mode of each curve.



589 **Figure 5. IL-2 preferentially expands clonotypes with a diabetes-related specificity.**
 590

591 **(A)** The proportion of CDR3s specific for cancer, EAE, SLE and diabetes found within
 592 the expanded clonotypes of each population (n=6). Box-and-whisker plots show the
 593 median and outliers. **(B)** CDR3s with a disease-related specificity were connected by

594 LD=1 to the pool of amTreg and nTreg CDR3s identified across the six IL-2 treated
595 NOD mice. The degree of connectivity, i.e the number of LD=1 edges connecting a given
596 node, of disease-specific CDR3s is plotted (n=52 in cancer, n=50 in EAE, n=49 in SLE
597 and n=52 in T1D). **(A, B)** Wilcoxon test was performed with the T1D group as a
598 reference: ns $p > 0.05$, * $P \leq 0.05$, ** $P \leq 0.01$ and *** $P \leq 0.001$. **(C)** Graphical
599 representation of the LD=1 networks in NOD AAV-IL-2 treated nTregs and amTregs.
600 Unconnected sequences are not shown. Identical sequences found in the database and
601 samples from IL-2 treated mice are shown in red, their neighbors in blue as well as
602 diabetes-related sequences from the database.